



# Optimum energy extraction from rotational motion in a parametrically excited pendulum

Krishnan Nandakumar<sup>a,\*</sup>, Marian Wiercigroch<sup>a</sup>, Anindya Chatterjee<sup>b</sup>

<sup>a</sup> Centre for Applied Dynamics Research, School of Engineering, University of Aberdeen, UK

<sup>b</sup> Department of Mechanical Engineering, Indian Institute of Technology Kharagpur, Kharagpur, India

## ARTICLE INFO

### Article history:

Received 14 May 2011

Received in revised form 12 March 2012

Available online 23 March 2012

### Keywords:

Parametric pendulum

Energy extraction

Period-1 rotation

Damping

## ABSTRACT

A pendulum rotating under vertical base excitation is considered from the viewpoint of energy extraction. Since the uncontrolled system can exhibit complex dynamics, we consider an added control torque and seek the optimal period-1 rotational motion for maximum energy extraction. We find, and confirm through complementary methods, that the limiting optimal motion for harmonic base excitation is piecewise-constant: there are extended dwells at the top and bottom positions with rapid transitions in between. The limiting optimal solution gives about a quarter more energy extraction than uniform rotation, in the limit of no damping. Approximating motions with finite-speed transitions can be almost as good. Base excitations other than pure sinusoids are also considered and the corresponding optima determined.

© 2012 Elsevier Ltd. All rights reserved.

## 1. Introduction and motivation

A pendulum is an archetype of strongly nonlinear dynamical systems. Pendulums with vertical base excitation (parametric forcing) exhibit rich dynamic behaviour and have been extensively studied from both theoretical and applied perspectives. Theoretical studies (Leven and Koch, 1981; Clifford and Bishop, 1995) have focused on constructing stability charts, and studying the bifurcation scenarios leading to rotational motions, equilibria, chaos and other complex responses. From an applied perspective, energy extraction from a base excited pendulum has been proposed. The dynamics of the damped, vertically excited pendulum (with various modifications) have been studied by a number of authors (Horton et al., 2011; Xu and Wiercigroch, 2007; Lenci et al., 2008; Xu et al., 2005). While our interest here is in energy extraction rather than bifurcation analysis, it may be worthwhile to consider the results of some of these previous studies to motivate the present work.

A schematic of the damped, parametrically excited pendulum is shown in Fig. 1 (left), wherein a vertical, harmonically varying displacement is applied to the pivot point. The dynamics of this system is governed by

$$\ddot{\theta} + \gamma\dot{\theta} + (1 + p \cos(\omega t)) \sin(\theta) = 0, \quad (1)$$

and was studied in detail by Xu et al. (2005). In Eq. (1),  $\gamma$  represents the viscous damping,  $p$  is the strength of parametric excitation, and  $\omega$  is the excitation frequency. It was observed in the work of Xu et al. (2005) that this system can exhibit a variety of dynamic behaviours such as period-1 oscillations, period-2 oscillations, period-1 rotations, period-2 rotations, oscillation-rotations, chaos, etc. Two such important motions, namely period-2 oscillations (one oscillation per two cycles of forcing) and period-1 rotations, are plotted in Fig. 1 (right) for different sets of parameters. Most importantly, such motions can co-exist in certain parameter regimes. For example, for the system of Eq. (1), period-2 oscillations and period-1 rotations co-exist for  $\gamma = 0.1$ ,  $p = 0.8$  and  $\omega = 2.1$ .

In this paper, we are interested in period-1 rotational motions of the pendulum, wherein the pendulum completes one rotation during one period of parametric forcing. However, the period-1 motions may not necessarily be stable. Even if the rotations are stable, there could be other co-existing motions such as oscillations with competing basins of attraction. Hence, in practical applications, active control is necessary to put the pendulum onto the desired period-1 rotation and stabilize that motion.

To illustrate this point more clearly, we briefly consider some studies of the system from the literature. The following summary of some of the complex dynamics of the uncontrolled vertically driven pendulum will serve to both emphasize the unavoidable need for control as well as the difficulty in selecting the most appropriate regime of operation.

A typical bifurcation diagram of the pendulum system of Fig. 1 from a recent study by Horton et al. (2011) is presented in Fig. 2. Herein, the X-axis represents excitation frequency, and the Y-axis represents excitation strength. The curves of interest here are the

\* Corresponding author. Tel.: +44 01224 267636.

E-mail addresses: [nandakumar.1979@gmail.com](mailto:nandakumar.1979@gmail.com) (K. Nandakumar), [m.wiercigroch@abdn.ac.uk](mailto:m.wiercigroch@abdn.ac.uk) (M. Wiercigroch), [anindya100@gmail.com](mailto:anindya100@gmail.com) (A. Chatterjee).

<sup>1</sup> Presently with Lloyd's Register, Aberdeen, UK.

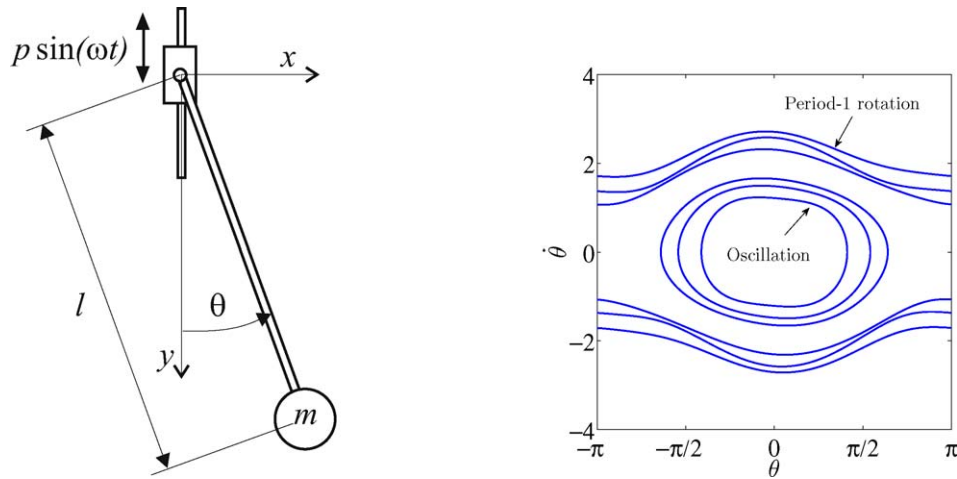


**Fig. 1.** Left: A schematic of a base excited, vertical pendulum. Right: Typical oscillation and period-1 rotation motions of Eq. (1) for different excitation strengths.

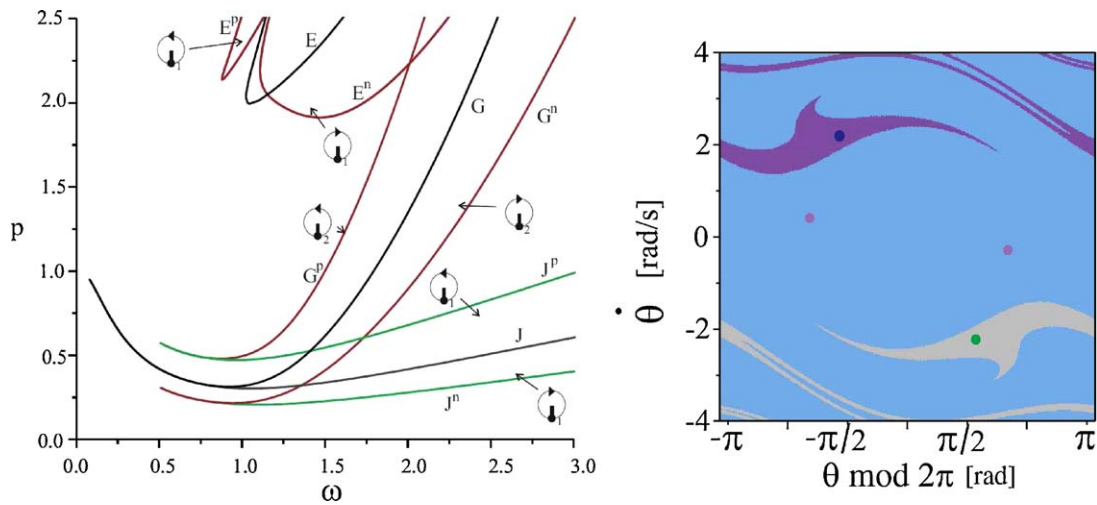


**Fig. 2.** Left: A typical bifurcation diagram for a damped parametrically excited pendulum in the excitation frequency-amplitude plane. The figure shows the existence and bifurcations of rotational motions. Of particular relevance are the black and grey curves E, G and J which indicate the bifurcations of the period-1 and period-2 rotational motions. Right: Basins of attraction on the phase plane with co-existence of rotation and oscillation motions (see text for further details). Both panels are adopted from Horton et al. (2011).

black and grey ones marked E, G and J in the figure. These curves indicate the bifurcations of the period-1 and period-2 rotations. In particular, for a fixed  $\omega$ , as the excitation strength  $p$  is increased from zero, the period-1 rotational motions are born on the curve J. These period-1 motions lose stability on the curve G and finally regain stability along the curve E. Thus, from Fig. 2, we can see that there exists a large region in the  $p$ - $\omega$  parameter space (between the curves G and E) wherein the period-1 rotation is unstable. Even in the region where the period-1 rotation is stable, there may co-exist other attractors and the basin of attraction of the desired motion may be relatively narrow. To illustrate, consider Fig. 2 (right) wherein the parameter combination of  $p=0.5$  and  $\omega=1.8$  is considered. A stable period-1 rotation exists for these parameter values (see Fig. 2 (left)). However, as seen in Fig. 2 (right), there exist four attractors for this parameter set and we will have to start in the appropriate basin to be able to reach the desired period-1 motion. It is thus clear that in practical applications of energy extraction, active control will be necessary.

In this paper, we consider the setting of a wave-energy extraction device idealized as a pendulum subjected to vertical base excitation from waves, wherein, from among the variety of periodic motions, period-1 rotational motions are established through

active control. In this setting, we ask the following question: *Which period-1 trajectory maximizes the energy extracted per cycle?*

The answer will shed light on fundamental limits on the maximum available energy per cycle that can be extracted from the pendulum in practical applications. We initially address the problem through a calculus of variations approach but obtain somewhat puzzling results, and then use approximate numerical optimization using truncated Fourier series with undetermined coefficients to obtain better understanding. We finally revisit the variational formulation with a small regularizing parameter, which gives results consistent with both of the previous solutions, and provides further understanding of the role played by damping. We close the paper with a discussion of non-sinusoidal excitations.

## 2. Solution using the calculus of variations approach

The actively-controlled pendulum system, i.e., with an applied torque  $T$  (which includes the control-torque, as well any sources of dissipation), is depicted in Fig. 3. The equation of motion of this pendulum system, after suitable non-dimensionalization, is

$$\ddot{\theta} - (1 + \delta \sin(\omega t)) \sin(\theta) = T(t), \quad (2)$$

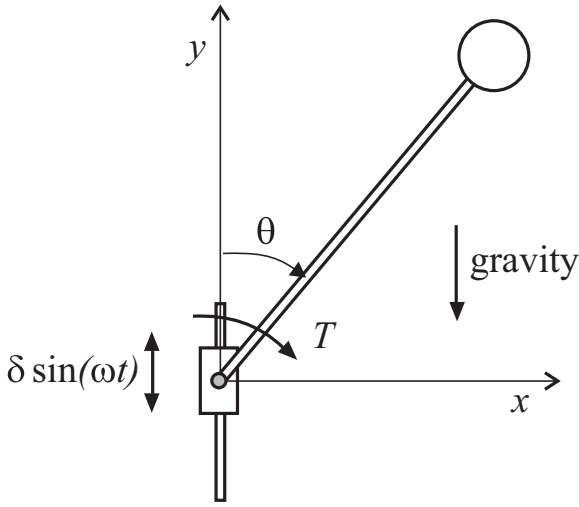


Fig. 3. A schematic of a base excited, vertical pendulum with applied torque.

where  $\theta$  is the angle made by the pendulum with the vertical,  $\delta$  is the non-dimensional base excitation amplitude,  $\omega$  is the non-dimensional excitation frequency, and  $T$  is the external torque (inclusive of damping, control torque, and other loads). Note that the form of Eq. (2) is slightly different from Eq. (1) due to the differences in the definition of  $\theta$  (see Figs. 1 (left) and 3).

We assume that the actively controlled pendulum executes period-1 rotations. More precisely

$$\theta\left(t + \frac{2\pi}{\omega}\right) = \theta(t) + 2\pi \quad (3)$$

$$\dot{\theta}\left(t + \frac{2\pi}{\omega}\right) = \dot{\theta}(t). \quad (4)$$

The average power output of the system is

$$P = \frac{\int_0^{2\pi/\omega} T d\theta}{2\pi/\omega}, \quad (5)$$

which can be rewritten as

$$P = \frac{\int_0^{2\pi/\omega} T \dot{\theta} dt}{2\pi/\omega}, \quad (6)$$

Utilizing Eq. (2), the objective function (representing power output) becomes

$$P = \frac{\omega}{2\pi} \int_0^{2\pi/\omega} (\ddot{\theta}\dot{\theta} - (1 + \delta \sin(\omega t)) \sin(\theta)\dot{\theta}) dt. \quad (7)$$

Note that the first term in the integrand is  $\int_0^{2\pi/\omega} \ddot{\theta}\dot{\theta} dt = \int_0^{2\pi/\omega} d(\dot{\theta}^2/2)$ , which vanishes owing to the periodicity requirements of Eq. (4). Thus our objective function becomes

$$P(\theta, \dot{\theta}) = -\frac{\omega}{2\pi} \int_0^{2\pi/\omega} (1 + \delta \sin(\omega t)) \dot{\theta} \sin(\theta) dt. \quad (8)$$

Actually, even the integral of  $\dot{\theta} \sin(\theta)$  over one period is zero. We are interested in the trajectory  $\theta(t)$  which minimizes  $P$ . Using routine variational calculus (e.g., Weinstock, 1974), we arrive at the following Euler–Lagrange equation governing the extremum trajectory

$$\delta\omega \cos(\omega t) \sin(\theta) = 0. \quad (9)$$

The extremum solutions given by Eq. (9) are  $\theta = n\pi$ . This means that the pendulum is at rest upright or hanging down unless  $\cos(\omega t) = 0$ .

To better understand the situation, we now turn to approximate numerical optimization using truncated Fourier series, and revisit Eq. (9) later.

### 3. Numerical optimization

Since we are interested in period-1 rotation solutions, we assume the following form for the solution:

$$\theta(t) = \omega t + a_0 + \sum_{n=1}^N (a_n \sin(n\omega t) + b_n \cos(n\omega t)). \quad (10)$$

Thus

$$\dot{\theta}(t) = \omega + \sum_{n=1}^N (n\omega a_n \cos(n\omega t) - n\omega b_n \sin(n\omega t)). \quad (11)$$

Using the above representation in Eq. (7), we numerically find the minimizing solution (i.e., solve for the coefficients  $a_0$ ,  $a_n$ s and  $b_n$ s) for given  $\delta$  and  $\omega$ . The numerical optimization is carried out in MATLAB using the FMINSEARCH routine. As a procedural information, during each function evaluation step in the optimization routine the integral of Eq. (7) was approximated by a finite summation over small time intervals. The function evaluation tolerance parameter TOLFUN is fixed at  $10^{-10}$  and TOLX is fixed at  $10^{-12}$ .

We choose four different combinations of excitation strengths and frequencies such that  $\omega$  is near the 1:2 resonance where there is high incidence of seeing period-1 rotations (see Xu et al., 2005). For these parameter sets, the optimization procedure is carried out for increasingly large values of  $N$  and the results are plotted in Fig. 4. In Fig. 4 and all further plots of optimal solutions in the paper, we choose the X-axis to be the non-dimensional time  $\tau = \omega t/2\pi$ . Thus over one forcing period  $\tau \in [0, 1]$ . Fig. 4 suggests that the Fourier series approximation converges to a piecewise constant solution, regardless of the specific excitation strength and frequency.

In this limiting piecewise constant solution, the pendulum alternately hangs down or stands upright, for half a period each time, making rapid (instantaneous) transitions ( $\pi$ -rotations) every time  $\cos(\omega t) = 0$ ; in particular, it is upright when  $\cos(\omega t) > 0$  and hangs downwards when  $\cos(\omega t) < 0$ , with  $\dot{\theta}$  positive at every transition. The infinite velocity during the transitions is unphysical, and is a consequence of our not having limited the maximum possible magnitude of the torque  $T$ . In practice, we may wish to make the transitions as rapid as mechanically feasible. What is important is that the limiting solution (as indicated by the finite dimensional approximation) matches the results obtained from the calculus of variations (Eq. (9)). We now return to the calculus of variations.

### 4. Variational calculation with a penalty on high velocities

In order to make the solution more realistic, we modify our objective function such that large velocities are penalized. The modified objective function is

$$\begin{aligned} \bar{P} = & \frac{\omega}{2\pi} \int_0^{2\pi/\omega} \dot{\theta}\dot{\theta} dt - \frac{\omega}{2\pi} \int_0^{2\pi/\omega} (1 + \delta \sin(\omega t)) \sin(\theta)\dot{\theta} dt \\ & + \frac{\omega}{4\pi} \int_0^{2\pi/\omega} \epsilon \dot{\theta}^2 dt. \end{aligned} \quad (12)$$

where  $0 < \epsilon \ll 1$  penalizes large velocities in the solution. The Euler Lagrange equation is

$$\epsilon \ddot{\theta} - \delta\omega \cos(\omega t) \sin(\theta) = 0. \quad (13)$$

The above is a singularly perturbed nonlinear Mathieu equation. We are interested in rotating solutions of the above equation, satisfying

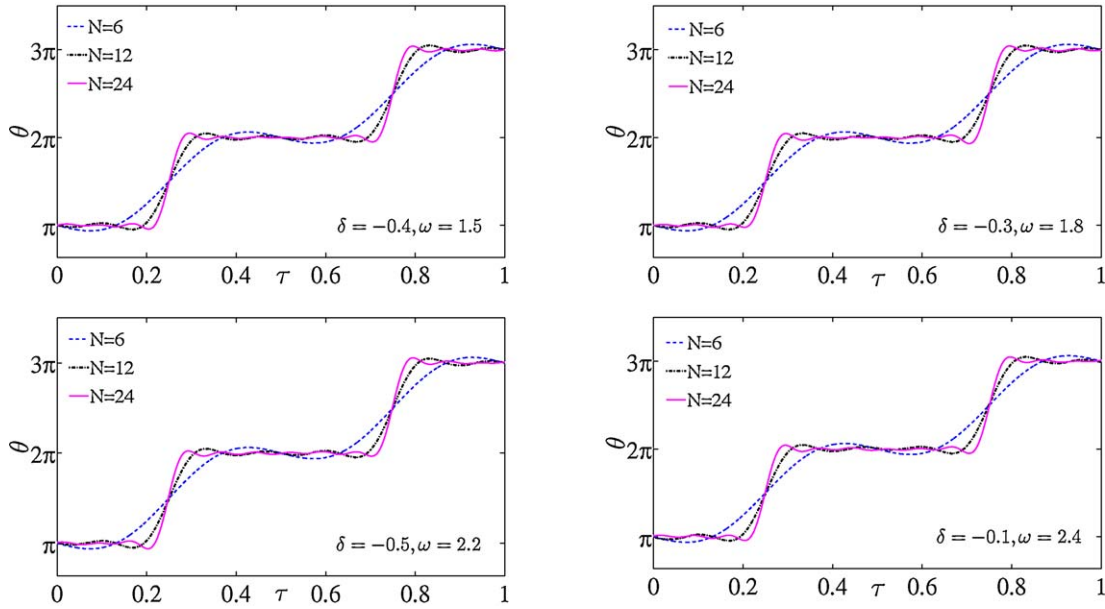


Fig. 4. Plot showing the results of numerical optimization for various combinations of  $\delta$  and  $\omega$ . It appears that as the number of harmonics,  $N$ , increases, the solutions approaches a piecewise constant solution immaterial of  $\delta$  and  $\omega$ .

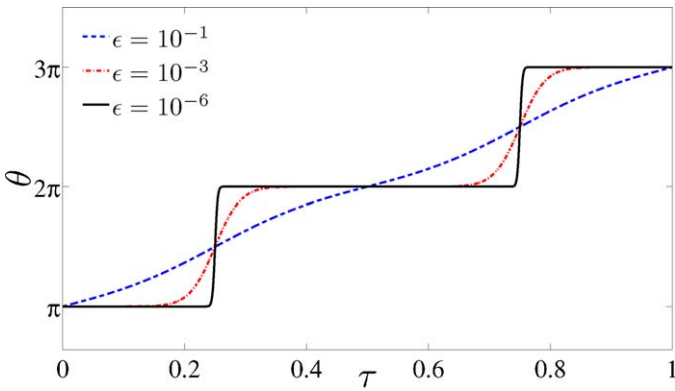


Fig. 5. Numerically obtained plots of the minimizing trajectory of Eq. (13) for different values of  $\epsilon$  with  $\delta = -0.3$  and  $\omega = 1.8$ .

Eqs. (3) and (4). In this paper, we have not attempted an analytical treatment of Eq. (13) (see Izmailov et al., 1995, for a linear system) and instead obtain the minimizing solutions numerically. All calculations are performed for  $\delta = -0.3$  and  $\omega = 1.8$ . Solutions were obtained using the BVP4C routine of MATLAB.

Three solutions, for progressively smaller  $\epsilon$  values, are plotted in Fig. 5. The approach to the limiting solution is clearly visible. Interestingly, for larger  $\epsilon$ , the solution approaches  $\theta = \omega t + \pi$ , which we take as the best steady-speed solution.

### 5. Damping and the penalty parameter

We found from the previous section that the introduction of a penalizing term in the objective function yields a smoother optimal solution. The penalizing term has, in addition, a useful physical interpretation which we clarify here.

Consider the pendulum system of Fig. 3, but with an explicitly added torsional viscous damping. The equation of motion after suitable non-dimensionalization is

$$\ddot{\theta} + \gamma \dot{\theta} - (1 + \delta \sin(\omega t)) \sin(\theta) = T(t), \tag{14}$$

where  $\gamma$  is the viscous damping coefficient. For this system the net power output that is extracted by the external torque is given by

$$\begin{aligned} \bar{W} = & \frac{\omega}{2\pi} \int_0^{2\pi/\omega} \dot{\theta} \dot{\theta} dt - \frac{\omega}{2\pi} \int_0^{2\pi/\omega} (1 + \delta \sin(\omega t)) \sin(\theta) \dot{\theta} dt \\ & + \frac{\omega}{2\pi} \int_0^{2\pi/\omega} \gamma \dot{\theta}^2 dt. \end{aligned} \tag{15}$$

On comparison of Eqs. (12) and (15), we find that the penalized objective function indeed corresponds to the work extracted from the system of Eq. (14), where the damping parameter is  $\gamma = \epsilon/2$ . Thus the penalty parameter introduced in Eq. (12) is related to the damping in the system which penalizes large velocities and yields a smoother optimal solution.

The introduction of damping, while smoothing the optimal solution, also dissipates energy. To estimate the optimum work output after losses to damping, we evaluate Eq. (15) for the optimum solution (obtained as before) for a range of values of the damping parameter  $\gamma$  and for  $\delta = -0.3$  and  $\omega = 1.8$ . Results are plotted in Fig. 6.

It is seen from Fig. 6 that for large damping values, no positive work is extracted. However, for progressively decreasing damping, we extract useful energy from the system. In particular, for the considered case of  $\delta = -0.3$  and  $\omega = 1.8$ , no useful energy extraction is possible for  $\gamma > 0.0856$ . Also, we observe from Fig. 6 that as the damping progressively decreases ( $\gamma \rightarrow 0$ ) the maximum energy output starts approaching a limiting value. For the plotted case of  $\delta = -0.3$  and  $\omega = 1.8$ , this limiting value is 0.3438, which equals the work obtained from the piecewise-constant solution, as discussed next.

### 6. Work extracted

Here, we compute and compare the maximum work that can be extracted from the undamped system for the three cases: uniform rotation, piecewise constant solution, and the Fourier series approximation to the piecewise constant solution. We recall that

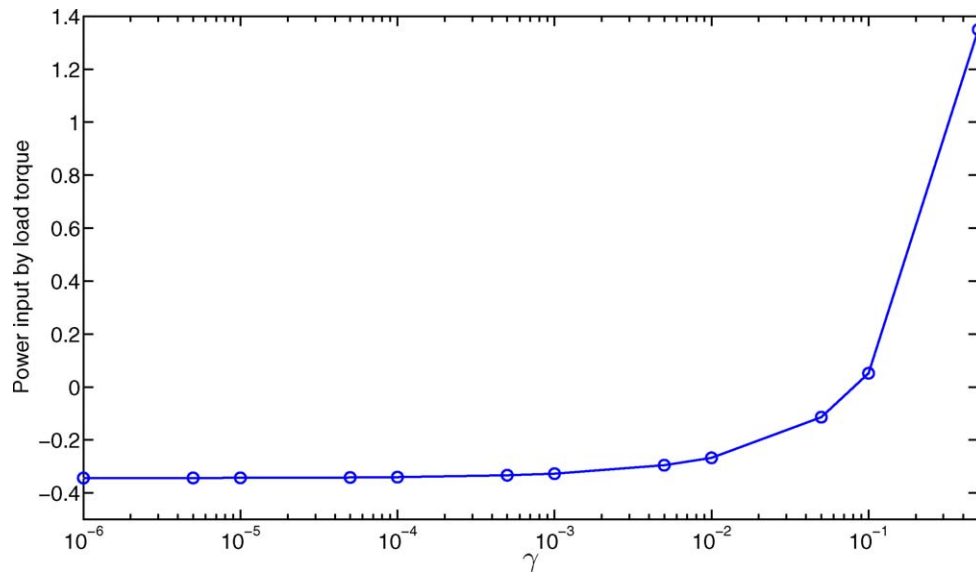


Fig. 6. A plot of the power input to the pendulum system in the presence of damping (note that negative power input indicated positive power output from the system).

the average power extracted per cycle (see Eq. (8)) is the negative of the work done by the external torque:

$$P = \frac{\omega}{2\pi} \int_0^{2\pi/\omega} (1 + \delta \sin(\omega t)) \dot{\theta} \sin(\theta) dt. \tag{16}$$

For the uniform rotation solution,  $\theta = \omega t + \pi$ . Substituting for  $\theta$  in Eq. (16), we obtain the maximum work extracted for the uniform rotation case as

$$-P = \frac{\omega\delta}{2}. \tag{17}$$

For the piecewise constant solution, the solution stays constant except near  $t = \pi/2\omega$ , and  $t = 3\pi/2\omega$ . In the boundary layer around  $t = \pi/2\omega$ ,  $\sin(\omega t) \approx 1$ , and in the boundary layer (or rapid transition region) around  $t = 3\pi/2\omega$ ,  $\sin(\omega t) \approx -1$ . Thus we have

$$P \approx \frac{\omega}{2\pi} \int_{(\pi/2\omega)-\alpha}^{(\pi/2\omega)+\alpha} (1 + \delta) \dot{\theta} \sin(\theta) dt + \frac{\omega}{2\pi} \int_{(3\pi/2\omega)-\alpha}^{(3\pi/2\omega)+\alpha} (1 - \delta) \dot{\theta} \sin(\theta) dt, \tag{18}$$

wherein we can take  $\alpha \rightarrow 0$  as  $\epsilon \rightarrow 0$ , and the quantity on the right hand side of Eq. (18) approaches the maximum work extracted from the limiting piecewise constant solution. Thus, for the piecewise constant solution, we obtain

$$-P = \frac{2\omega\delta}{\pi}, \tag{19}$$

which exceeds the amount of Eq. (17) by 27.32%.

We also obtain the maximum work output for the Fourier series approximation of Eqs. (10) and (11) from the numerical optimization routine. For the considered case of  $\delta = -0.3$  and  $\omega = 1.8$ , we present the results for these three cases in Table 1. One can verify

**Table 1**  
Comparison of maximum power extracted per cycle from the cases of uniform rotation, piecewise constant rotation, and Fourier series approximation.

Case	Maximum work output
Uniform rotation	0.2700
Fourier series with 24 terms	0.3424
Piecewise constant solution	0.3438

that even a one-harmonic correction to the constant speed solution can give a power output increase of about 22%, with relatively gentler accelerations. However, there are small velocity reversals within the cycle.

### 7. Effects of non-harmonic excitation

#### 7.1. Smooth periodic, but non-harmonic, excitation

Until now, we have focused on the case when the base excitation is purely harmonic. It is interesting, however, to examine the case when the excitation (base acceleration) is a general periodic function  $q(t)$  rather than harmonic, and determine the nature of the resulting optimum solution and the corresponding optimum work output. Thus our governing equation becomes

$$\ddot{\theta} - (1 + q(t)) \sin(\theta) = T(t), \tag{20}$$

where  $q(t)$  is a periodic function such that

$$q\left(t + \frac{2\pi}{\omega}\right) = q(t).$$

The Euler–Lagrange equation governing the optimal solution becomes

$$\dot{q}(t) \sin(\theta) = 0, \tag{21}$$

and the corresponding equation obtained after penalizing large velocities is

$$\epsilon \ddot{\theta} - \dot{q}(t) \sin(\theta) = 0. \tag{22}$$

From Eq. (21) it is clear that in the optimal solution  $\theta = 0$  or  $\pi$  when  $\dot{q} \neq 0$ . However, since we also require the pendulum to complete a revolution in one period of the forcing,  $\theta$  changes at the instants when  $\dot{q} = 0$ . We will examine these effects first for a periodic excitation with two harmonics, and then consider the slightly complicated case of square-wave base excitation. More specifically, let

$$q(t) = \delta \left( \sin(\omega t) + \frac{1}{4} \sin(2\omega t) \right), \tag{23}$$

and for this choice of  $q(t)$  and for  $\omega = 1.8$  and  $\delta = -0.3$ ,  $\dot{q}$  vanishes at the normalized time instants  $\omega t_1/2\pi = 0.1903$  and  $\omega t_2/2\pi = 0.8096$ . For this choice of  $q(t)$ , we compute the optimal solution through our Fourier-series based numerical optimization routine and plot the

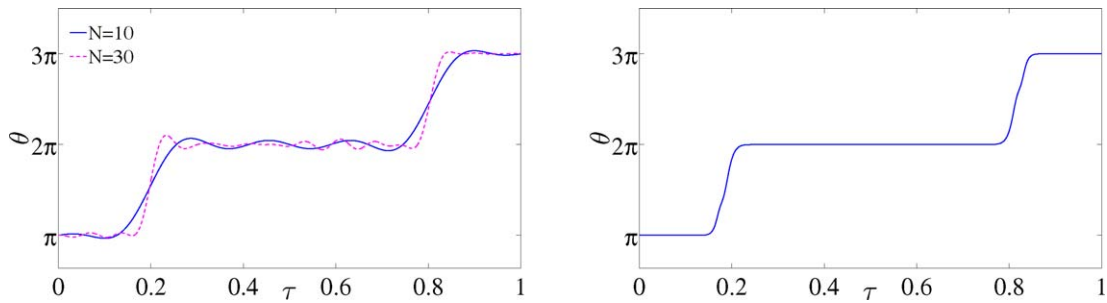


**Fig. 7.** Left: Plot showing the results of numerical optimization for the case with the excitation as in Eq. (23) with  $\delta = -0.3$  and  $\omega = 1.8$ . It appears that as the number of harmonics,  $N$ , increases, the solutions approach a piecewise constant solution, and the time instants during which  $\theta$  undergoes rapid changes correspond to the instants when  $\dot{q} = 0$  (see text for details). Right: Numerically obtained plots of the minimizing trajectory of Eq. (22) for  $\epsilon = 1e^{-4}$  and with  $\delta = -0.3$  and  $\omega = 1.8$ . The closeness of the solution to the piecewise constant solution is clear. The transition points involving rapid changes in  $\theta$  coincide with the instants during which  $\dot{q}$  vanishes.

**Table 2**  
Comparison of maximum power extracted per cycle, for non-harmonic excitation of Eq. (23) with  $\delta = -0.3$  and  $\omega = 1.8$ .

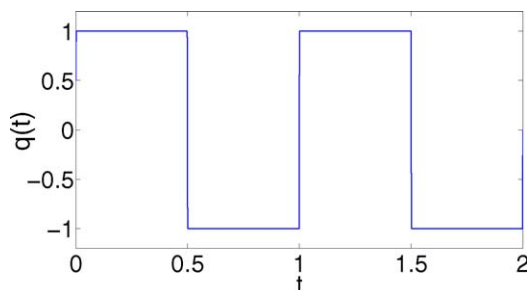
Case	Maximum work output
Uniform rotation	0.2700
Fourier series with 30 terms	0.3763
Piecewise constant solution	0.3784

results for numbers of retained harmonics in Fig. 7 (left). We also compute the optimal solution for the penalty-based formulation of Eq. (22), for  $\epsilon = 1e^{-4}$  and plot the result in Fig. 7 (right).

Finally, we compute the optimum work extracted per cycle from the optimum piecewise constant solution in this case and compare the same with the work obtained from a uniform rotation solution. It can be shown that (following the calculations outlined in the previous section), if  $t_1$  and  $t_2$  are the instants when  $\dot{q}$  vanishes, then the optimum work extracted is given by

$$-P = \frac{\omega\delta}{\pi} [\sin(\omega t_2) - \sin(\omega t_1)] + \frac{\omega\delta}{4\pi} [\sin(2\omega t_2) - \sin(2\omega t_1)]. \quad (24)$$

The work output from the uniform rotation solution  $\theta = \omega t + \pi$  is still given by Eq. (17). In Table 2 we give a comparison of the work output from the uniform rotation solution, the piecewise constant solution as well as from the approximate optimum solution through our truncated Fourier series optimization routine in Table 2. It is seen that in this case the optimal work output is approximately 40% greater than that obtained from uniform rotation solution. We observed that in this case of excitation with two sinusoids, the optimal work output in relation to the uniform rotation solution is higher than the pure harmonic case presented earlier. This points to an interesting academic question of *what* base excitation results in maximum extraction, which we leave to future work.



7.2. Square wave excitation

We finally consider the case of a square wave acceleration applied as a parametric base excitation to the pendulum. The discontinuous nature of the square wave excitation leads to some subtleties which we explain here. For ease of explanation, we plot a unit square wave excitation in Fig. 8 (left). It is clear that  $\dot{q} = 0$  for all instants except the transition instants during which  $\dot{q}$  is not defined (or infinitely large). Proceeding with the Euler-Lagrange equation as before (and temporarily ignoring the non-differentiability of  $q(t)$  during the transition instants) we get

$$\dot{q}(t) \sin(\theta) = 0. \quad (25)$$

Since  $\dot{q} = 0$  for all instants where defined, it is clear that the above equation is identically satisfied for almost all time. There are no restrictions on the optimal solution for most of the duration of the forcing cycle. At the instants when  $\dot{q}$  grows infinitely large, the Euler-Lagrange equation is still satisfied if  $\sin(\theta) = 0$ . Thus the optimal solution for the case of square wave excitation is *non-unique* with the constraint that all the possible solutions have to satisfy  $\sin(\theta) = 0$  during the instants when the excitation reverses its sign.

To verify the above conclusions, we proceed with our numerical optimization routine. However we first approximate the square wave excitation by a smooth approximation. Specifically we approximate the square wave excitation over one period using the following form

$$H(t) \approx \tanh\left[\frac{t - (2\pi/\omega)}{\alpha}\right] - \tanh\left[\frac{t - (\pi/\omega)}{\alpha}\right] + \frac{1}{2} \tanh\left[\frac{t}{\alpha}\right] - \frac{1}{2} \tanh\left[-\frac{t}{\alpha}\right], \quad (26)$$

where  $\alpha$  is a small, control parameter. For  $\omega = 1.8$ , the original square-wave and the approximation as specified in Eq. (26) are plotted in Fig. 8 (right) for decreasing values of  $\alpha$ . It is seen that

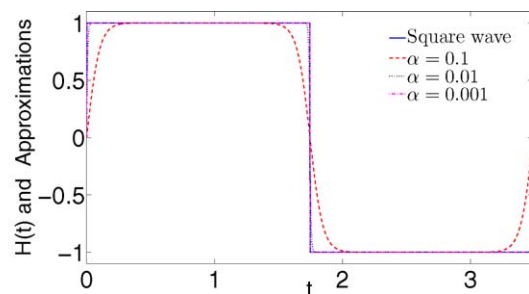


**Fig. 8.** Left: Representative unit square wave excitation for explanation purposes. Right: Unit square wave excitation with an angular frequency of  $\omega = 1.8$  as considered in the text and its approximations by hyperbolic tangent functions over one period of excitation.

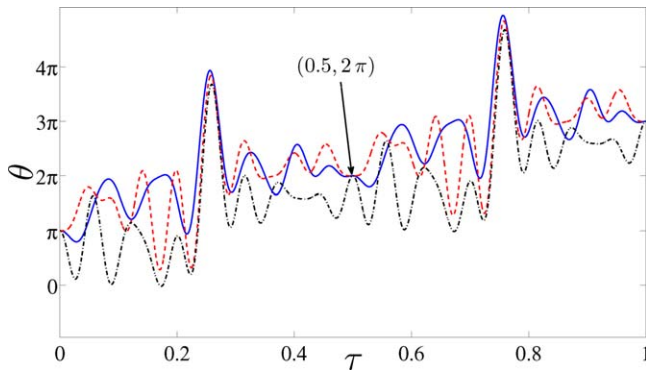


**Fig. 9.** Non-unique optimal solutions obtained from the numerical optimization routine for the case of square wave excitation with  $\delta = -0.3$  and  $\omega = 1.8$ . Square wave excitation is approximated using Eq. (26) with  $\alpha = 0.001$ . All the solutions pass through  $(0.5, 2\pi)$  such that  $\sin(\theta) = 0$  at the instant when the square wave changes sign.

$\alpha = 0.001$  approximates the original square wave very well. We now proceed with the numerical optimization procedure. All the simulations are done for  $N = 40$  harmonics, with the square wave excitation over one period being approximated according to Eq. (26) and the control parameter fixed at  $\alpha = 0.001$ . As discussed earlier, the constant nature of the square wave excitation during most of the time period results in non-unique solutions for optimum work output. Our numerical optimization routine returned essentially identical (up to 6 decimal places) work output for each of these solutions. Three such solutions obtained from the numerical optimization routine are plotted in Fig. 9 where the computed solutions differ in the normalized time intervals  $[0, 0.5)$  and  $[0.5, 1.0)$ . These intervals correspond to the constant values of the excitation (i.e.  $\dot{q} = 0$ ). At  $\tau = 0.5$ , the excitation changes rapidly ( $\dot{q} \neq 0$ ) and to satisfy Eq. (25) at this instant the solutions attain  $\theta = 2\pi$  such that  $\sin(\theta) = 0$ .

The variational equation for the optimum solution on penalizing large velocities reads as

$$\epsilon \ddot{\theta} - \dot{q}(t) \sin(\theta) = 0. \tag{27}$$

For the square wave case in the normalized time intervals  $[0, 0.5)$  and  $[0.5, 1.0)$ , Eq. (27) becomes

$$\epsilon \ddot{\theta} = 0. \tag{28}$$

The solution to the above represents a uniform rotation of the form

$$\theta(t) = \omega t + \pi. \tag{29}$$

The uniform rotation solution is such that  $\theta = 2\pi$  at the instant  $t = \pi/\omega$ . Note that the above solution is valid for  $\epsilon \neq 0$ . Thus the introduction of penalization has removed the non-uniqueness and chosen the uniform rotation solution among all the candidates. To confirm these observations, the boundary problem associated with Eq. (27) is solved, again approximating the square wave using the approximation as in Eq. (26). The results from the penalty formulation for progressively decreasing values of  $\alpha$  are plotted in Fig. 10. All the results are computed with  $\epsilon = 0.001$ ,  $\delta = -0.3$  and  $\omega = 1.8$ . The solutions are seen to approach the uniform rotation solution which is the straight line passing through the point  $(0.5, 2)$ .

The optimum work output for the square wave excitation case is now computed using the uniform rotation solution. We have for the optimum work output per cycle

$$P = \frac{\omega}{2\pi} \int_0^{2\pi/\omega} (1 + \delta q(t)) \dot{\theta} \sin(\theta) dt. \tag{30}$$

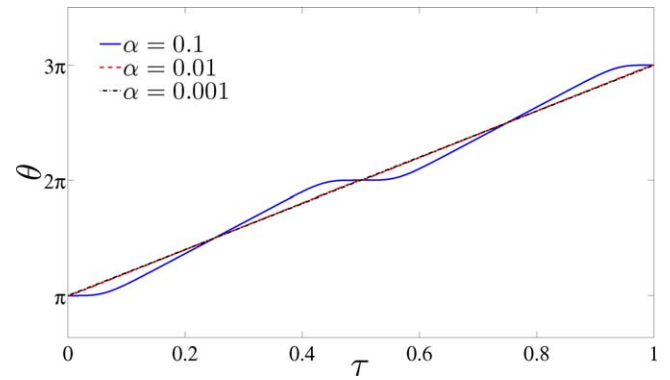


**Fig. 10.** Optimum solutions obtained from the penalty formulation Eq. (27) for the case of square wave excitation with  $\epsilon = 0.001$ ,  $\delta = -0.3$  and  $\omega = 1.8$ . Square wave excitation is approximated using Eq. (26), and solutions obtained for various values of  $\alpha$  are plotted. Solutions are approaching a uniform rotation solution passing through  $(0.5, 2\pi)$ .

**Table 3**

Comparison of maximum power extracted per cycle, for the case of square wave excitation with  $\delta = -0.3$  and  $\omega = 1.8$ , from the cases of uniform rotation, and the solutions from numerical optimization and by direct evaluation of the work integrals. In the case of square wave excitation, as explained in the text, there is non-uniqueness in the optimal solutions and uniform rotation is also a valid optimal solution. Thus the work output in this case is identical for the various cases.

Case	Maximum work output
Uniform rotation	0.3438
Fourier series with 40 terms	0.3438
Direct evaluation of Eq. (32)	0.3438

For the square wave case, using the uniform rotation solution as the optimal solution (for simplicity, although all non-unique solutions yield essentially the same answer), we have

$$P = -\frac{\omega^2}{2\pi} \int_0^{\pi/\omega} (1 + \delta) \sin(\omega t) dt - \frac{\omega^2}{2\pi} \int_{\pi/\omega}^{2\pi/\omega} (1 - \delta) \sin(\omega t) dt, \tag{31}$$

whereby

$$P = \frac{2\omega\delta}{\pi}. \tag{32}$$

For  $\delta = -0.3$  and  $\omega = 1.8$ , the optimum work extracted per cycle for the uniform rotation solution, from the various non-unique solutions given by the optimization routine, and from Eq. (32) are given in Table 3. It is seen in this case that the work output from the uniform rotation solution is identical to that obtained from the other non-unique optimal solutions.

Thus from the studies with two cases of excitation considered in this section, we conclude that the gain in the work output as given by the optimal solution over the uniform rotation solution is dependent on the nature of excitation.

### 8. Conclusions

We have sought, and found, the optimal angular motion of an actively controlled vertically and periodically driven pendulum with the aim of maximum work extraction. The optimal solution for typical base excitation and in the undamped limit, somewhat surprisingly, involves periods of vertical dwell interrupted by instantaneous half-rotations. The optimal trajectory for a harmonic base excitation gives a power output gain of about 27%. Somewhat smoother approximations to

the optimal trajectory give almost as good improvements in power output. Beyond some maximal level of viscous damping for any given forcing parameters, energy extraction is not possible.

Changing the nature of base excitation can change the net output. Non-zero sized intervals of constant base excitation lead to non-uniqueness in the optimal motion but, in the situation studied, not in the optimal power output.

This has been a purely theoretical study, and practical realization of these motions in actual wave-energy extraction devices may be taken up in future work.

### Acknowledgement

We thank the anonymous reviewers for helpful and insightful comments which have improved the technical merit of this paper.

### References

- Leven, R.W., Koch, B.P., 1981. Chaotic behaviour of a parametrically excited damped pendulum. *Physics Letters A* 86A (2), 71–74.
- Clifford, M.J., Bishop, S.R., 1995. Rotating periodic orbits of the parametrically excited pendulum. *Physics Letters A* 201, 191–196.
- Horton, B., Sieber, J., Thompson, J.M.T., Wiercigroch, M., 2011. Dynamics of the nearly parametric pendulum. *International Journal of Non-linear Mechanics* 46, 436–442.
- Xu, X., Wiercigroch, M., 2007. Approximate analytical solutions for oscillatory and rotational motion of a parametric pendulum. *Nonlinear Dynamics* 47, 311–320.
- Lenci, S., Pavlovskaia, E.E., Rega, G., Wiercigroch, M., 2008. Rotating solutions and stability of parametric pendulum by perturbation method. *Journal of Sound and Vibration* 310, 243–259.
- Xu, X., Wiercigroch, M., Cartmell, M.P., 2005. Rotating orbits of a parametrically-excited pendulum. *Chaos, Solitons, and Fractals* 23, 1537–1548.
- Weinstock, R., 1974. *Calculus of Variations with Applications to Physics & Engineering*. Dover publications, Inc., New York.
- Izmailov, A.F., Arnold, S., Holler, S., Myerson, A.S., 1995. Microparticle driven by parametric and random forces: Theory and experiment. *Physical Review E* 52 (2), 1325–1332.